Hindawi
Geofluids
Volume 2018, Article ID 1210950, 15 pages
https://doi.org/10.1155/2018/1210950

Research Article

New Understanding of Transient Pressure Response in the Transition Zone of Oil-Water and Gas-Water Systems

Wenbin Xu,[1] Zhihui Liu,[2] Jie Liu,[2] and Yongfei Yang[2]

[1]*Sinopec International Petroleum E&P Corporation, Beijing, China*
[2]*Research Centre of Multiphase Flow in Porous Media, China University of Petroleum (East China), Qingdao 266580, China*

Correspondence should be addressed to Yongfei Yang; yangyongfei@upc.edu.cn

Received 7 April 2018; Revised 7 July 2018; Accepted 29 July 2018; Published 17 September 2018

Academic Editor: Bisheng Wu

Well test analysis requires a preselected model, which relies on the context input and the diagnostic result through the pressure logarithmic derivative curve. Transient pressure outer boundary response heavily impacts on the selection of such a model. Traditional boundary-type curves used for such diagnostic purpose are only suitable for single-phase flow in a homogeneous reservoir, while practical situations are often much more complicated. This is particularly true when transient pressure is derived during the field development phase, for example, from permanent down-hole gauge (PDG), where outer boundary condition such as an active aquifer with a transition zone above it plays a big role in dominating the late time pressure response. In this case, capillary pressure and the total mobility in the transition zone have significant effect on the pressure response. This effect is distinctly different for oil-water system and gas water system, which will result in the pressure logarithmic derivatives remarkably different from the traditional boundary-type curves. This paper presents study results derived through theoretical and numerical well testing approaches to solve this problem. The outcome of this study can help in understanding the reservoir behavior and guiding the management of mature field. According to the theoretical development by Thompson, a new approach was derived according to Darcy's law, which shows that pressure response in the transition zone is a function of total effective mobility. For oil-water system, the total effective mobility increases with an increase in the radius of transition zone, while for gas-water system, the effect is opposite.

1. Introduction

With the increased reliability and technology enhancement, more and more PDG have been installed in oilfields around the world. Long-term data from PDG have the potential to provide more information about a reservoir than data from traditional pressure transient tests [1–3]. In particular, during the oil field development stage, the influence of multiphase flow due to long-term nature of PDG data is significant [4–6].

Some researchers proposed different scale models to study different types of reservoirs, such as fractured tight reservoirs [7, 8], preferential flow path with non-Darcy flow reservoirs [9], mature waterflooding reservoirs [10], and shale gas reservoirs [11, 12]. It is well known that the pressure logarithmic derivative curve has been used to identify true boundary model, but for multiphase flow well testing [13, 14], it is much more complicated, there is a great influence on pressure derivative due to the changes of fluid properties in the transition zone [15–17]. For example, the logarithmic derivative of bottom-hole pressure goes up and then goes down in the late time for gas-water reservoir systems with an active aquifer underneath. If using a traditional boundary-type curve for the model diagnostic, the wrong conclusions may be obtained.

In the literature, some articles have been published on multiphase flow, including those from Ramakrishnan and Wilkinson [18], Thompson (1997), and Roadifer [19]. Ramakrishnan and Wilkinson took account of Buckley-Leverett theory to describe the saturation profile and developed the radial Buckley-Leverett model [18]. Thompson examined the behavior of transient pressure for single-phase flow and multiphase flow in heterogeneous reservoirs. He used mass conservation equations and Darcy's law to

derive the pressure derivatives, which can be used to interpret well test from single-phase and multiphase flow. For single-phase gas reservoir, the pressure derivative is a function of the changing of rates with time. But for multiphase flow, Thompson focused on gas-condensate reservoir and water injection in an oil reservoir. He found that multiphase flow drawdown is heavily influenced by the mobility in the region, where the mobility is changing most rapidly with time. But for both oil-water and gas-water systems, Thompson did not consider the influence of transition zone [13].

Roadifer [19] examined the pressure behavior in a multiphase reservoir with a constant pressure boundary. Buckley-Leverett theory was used to analyze multiphase well test at the same time. Some laws on water saturation front were derived numerically. Roadifer used Thompson equation to interpret the pressure derivative of oil-water and oil-gas systems with constant pressure boundary. But he did not consider the influence of capillary pressure [19].

In fact, for multiphase flow system, capillary pressure cannot be ignored [20, 21]. In this work, based on Thompson equation, but also considering capillary pressure, a new theoretical equation is derived from Darcy's law, which shows that the pressure response in the transition zone is a function of total effective mobility and capillary pressure.

In order to study the rules of multiphase flow in transition zone, a 3D model was set up using Eclipse to simulate the pressure responses due to multiphase flow. The oil-water and gas-water systems were studied. Capillary pressure was considered under closed reservoir or constant pressure outer boundaries. Numerical well testing results can be interpreted qualitatively by this new theoretical equation for different multiphase reservoir systems. It is particularly useful for analyzing the transient pressure outer boundary response.

2. Theory

According to the law of conservation of matter for black oil system, isothermal multiphase flow in radial homogeneous reservoir is described by a partial differential equation [22], that is, diffusivity equation. When the conservation of mass equation in each flowing phase is satisfied, Darcy's law, which describes pressure losses of system, is also satisfied.

First, in an oil-water system, capillary pressure is considered and gravity effect is ignored. The production rate can be written at any radial location as [23–25]

$$q_t(r,t) = q_o(r,t) + q_w(r,t), \tag{1}$$

$$q_o(r,t) = \frac{KK_{ro}(S_w)}{\mu_o} A(r) \frac{\partial P_o}{\partial r}, \tag{2}$$

$$q_w(r,t) = \frac{KK_{rw}(S_w)}{\mu_w} A(r) \frac{\partial (P_o - P_c)}{\partial r}, \tag{3}$$

where $A(r)$ is the cross-sectional flow area, ft^2, that is, $A(r) = 2\pi rh$.

P_c is capillary pressure, psi, that is, $P_c = P_o - P_w$.

Equations (1), (2), and (3) can be rearranged as

$$\frac{\partial P_o}{\partial r} = \frac{q_t(r,t)}{2\pi rKh\lambda_t(r,t)} + \left[\frac{\lambda_w(r,t)}{\lambda_t(r,t)}\right] \frac{\partial P_c}{\partial r}, \tag{4}$$

where $\lambda_t(r,t)$ is the total effective mobility, that is, $\lambda_t(r,t) = \lambda_o(r,t) + \lambda_w(r,t) = (K_{ro}(S_w)/\mu_0) + (K_{rw}(S_w)/\mu_w)$.

Equation (4) can be applied to bounded reservoirs (outer boundary condition: $\partial P_e/\partial r|_{r=r_e} = 0, t > 0$, where r_e is the radial extent of reservoir and P_e is the pressure of outer boundary) or infinite-acting reservoirs (outer boundary condition: $\lim_{r\to\infty} P(r,t) = P_i$, where P_i is the initial reservoir pressure).

Considering finite-acting reservoirs, separating variables of (4) and taking integral along a radial direction:

$$\begin{aligned}\int_{r_w}^{r_e} \frac{\partial P_o}{\partial r} dr = {} & \frac{1}{2\pi Kh} \int_{r_w}^{r_e} \frac{q_t\left(r',t\right)}{r'\lambda_t\left(r',t\right)} dr' \\ & + \int_{r_w}^{r_e} \lambda_{\text{equivalent}}\left(r',t\right) \frac{\partial P_c}{\partial r'} dr',\end{aligned} \tag{5}$$

where $\lambda_{\text{equivalent}}(r',t) = \lambda_w(r',t)/\lambda_t(r',t)$.

The drawdown solution can be obtained from (5):

$$\begin{aligned}\Delta P_o(t) = {} & P_i - P_{wf}(t) \\ = {} & \frac{1}{2\pi Kh} \int_{r_w}^{r_e} \frac{q_t\left(r',t\right)}{r'\lambda_t\left(r',t\right)} dr' \\ & + \int_{r_w}^{r_e} \lambda_{\text{equivalent}}\left(r',t\right) \frac{\partial P_c}{\partial r'} dr'.\end{aligned} \tag{6}$$

Finally, according to the results of laboratory experiments, capillary pressure is a function of water saturation and water saturation is a function of radial distance and elapsed time. With respect to the natural logarithm of elapsed time, (6) can be differentiated, and the pressure derivative is given by

$$\begin{aligned}\frac{d\Delta P_o(t)}{d\ln t} = {} & \frac{1}{2\pi Kh} \int_{r_w}^{r_e} \left\{ \left[\frac{1}{r'\lambda_t\left(r',t\right)} \frac{\partial q_t\left(r',t\right)}{\partial \ln t}\right] \right. \\ & \left. - \frac{q_t\left(r',t\right)}{r'\lambda^2{}_t\left(r',t\right)} \frac{\partial \lambda_t\left(r',t\right)}{\partial \ln t} \right\} dr' \\ & + \int_{r_w}^{r_e} \frac{\partial \lambda_{\text{equivalent}}\left(r',t\right)}{\partial \ln t} \\ & \cdot \frac{\partial P_c\left(r',t\right)}{\partial S_w} \frac{\partial S_w\left(r',t\right)}{\partial r'} dr'.\end{aligned} \tag{7}$$

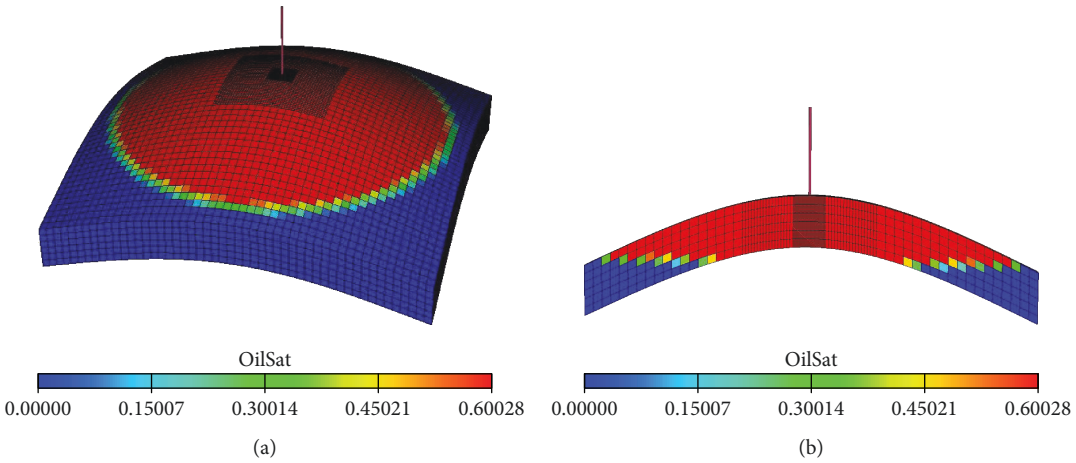

Figure 1: The anticline model: 3D (a) and 2D cross-section profile (b).

Equation (7) is the general equation, which applies to a radial flow system producing under defined wellbore boundary conditions.

From this equation, it can be seen that the pressure logarithmic derivative is a function of the total effective mobility, capillary pressure, liquid rate, and water saturation. Because this equation is highly nonlinear, an analytical solution cannot be obtained. So the numerical well testing approach was used to study multiphase flow rules, which considered phase effective permeability, capillary pressure, saturation gradient, and complex formation properties. The numerical results can be analyzed qualitatively by (7).

3. Numerical Well Testing

In this section, a 3D model was built to simulate multiphase flow in order to derive numerical solution. At the same time, (7) was used to verify qualitatively the accuracy of the numerical solution.

3.1. Numerical Model. In the constructed numerical model, the basic simulation grid consisted of 51 cells in the I-direction and 51 cells in the J-direction, with 6 layers (in both the anticline model and the flat model) (Figure 1). For the anticline model, the angle of formation bedding (α) is about 2.8° and much smaller, so the gravity of liquid can be neglected. Two systems, an oil-water model and a gas-water model, with different properties were used in the simulations. Data for the simulation model are summarized in Table 1.

3.1.1. Grid Description. Corner point geometry grids were used with approximate dimension of $200 \times 200 \times 30$ ft. Since bottom-hole pressure is sensitive to the size of grid, a nested grid technique was used in the model (Figure 2). This not only makes the wellbore better connected to the grid thereby avoiding numerical dispersion but also improves the simulation speed.

3.1.2. Fluid Characterization. The variation of the fluid properties in the lateral and vertical directions has been taken into account. Under reservoir pressure, the viscosity of gas, oil, and water for base model is 0.02 cp, 10 cp, and 0.5 cp, respectively.

Table 1: Reservoir model characteristics.

Parameter	Oil-water	Gas-water
Porosity Φ, %	30	30
Absolute permeability K, mD	500	10
Wellbore radius r_w, ft	0.15	0.15
Total reservoir thickness, ft	180	180
Initial reservoir pressure P_i, psi	2555	2430
Top depth, ft	4500	4500

3.1.3. Relative Permeability Modeling. Two sets of relative permeability data to oil-water model (Figure 3) and gas-water model (Figure 4) were used, which show that when K_{ro} is equal to K_{rw}, the corresponding water saturation is more than 0.5, which denotes that the rock has water wetting property.

3.2. Case Study 1: Oil-Water System. The studies were designed to test the impact of reservoir and fluid properties on the pressure response. All cases are the start of a single producer at a constant flow rate. These key parameters are listed in Table 2.

3.2.1. Single-Phase Flow. The first case considered single-phase flow. As shown in Figure 5, these are simulation results of the drawdown (DD) tests for closed system. The pressure derivatives of the two cases from flat and anticline models are the same. It means that the shape of model does not affect the numerical solutions of models.

For single-phase flow in these closed systems, mobility does not change and capillary pressure is not present, that is, $(\partial \lambda_t(r,t))/\partial t = 0$ and $P_o = P_w, P_c = 0$; therefore, (7) reduces to

$$\frac{d\Delta P_o(t)}{d(\ln t)} = \frac{t}{2\pi K h} \int_{r_w}^{r_e} \frac{1}{r' \lambda_t\left(r', t\right)} \frac{\partial q_t\left(r', t\right)}{\partial t} dr'. \quad (8)$$

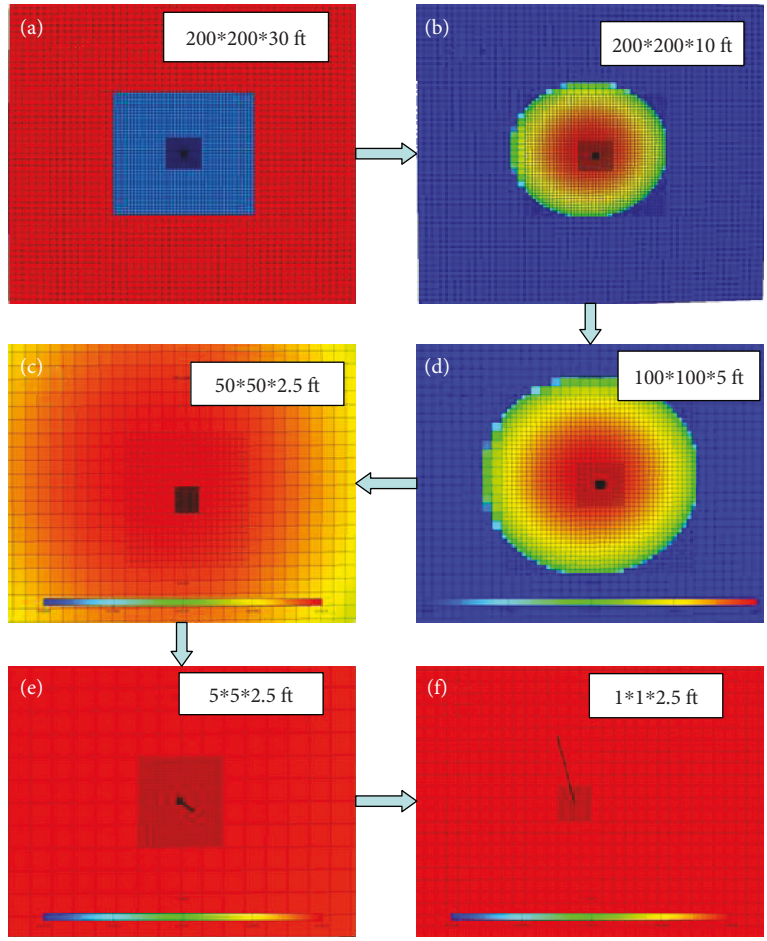

Figure 2: The procedure of nested grid systems, in which the size of the grid cells in each direction can be reduced step by step until the size of the near wellbore grid cells is close to the radius of the wellbore. (a) The basic configuration of nested grid systems. (b–f) The distribution of oil saturation, which indicates that the size of nested grid cells will be reduced from 200 ∗ 200 ∗ 10 ft to 1 ∗ 1 ∗ 1.5 ft.

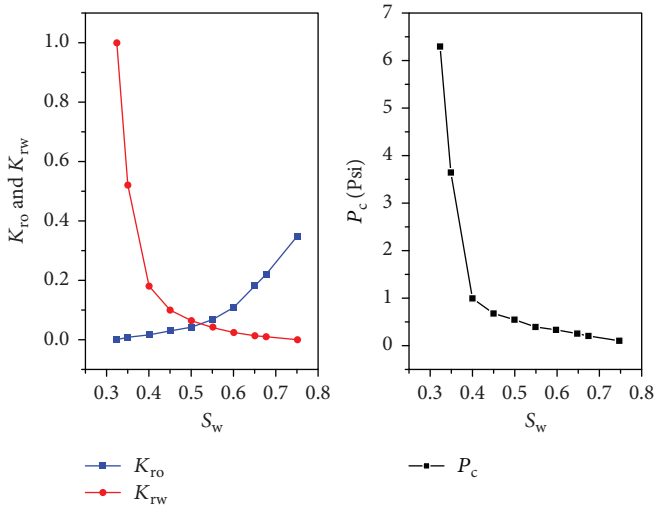

Figure 3: The oil/water relative permeability curve and capillary pressure.

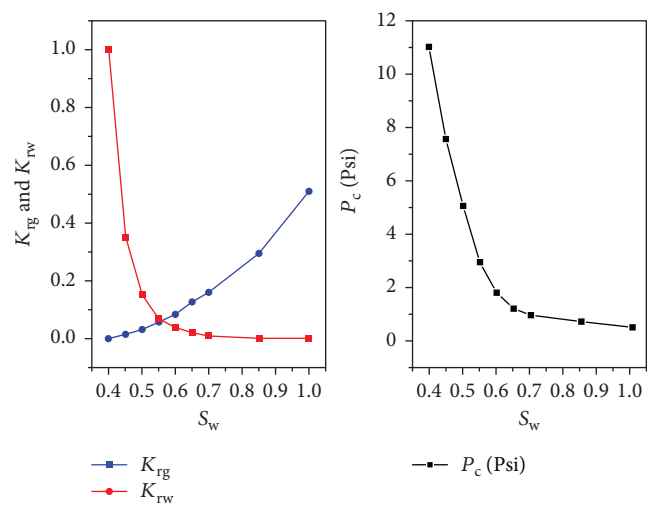

Figure 4: The gas/water relative permeability curve and capillary pressure.

Table 2: The designs of different flow conditions.

Fluid	Case	P_c	Model	OWC (ft)	Well location	Boundary condition	Oil viscosity (cp)
Single-phase model	Flat	/	Flat	/	Center	Closed system	10
	Anticline	/	Anticline	/	Center	Closed system	10
Oil-water model	OW-1	No P_c	Anticline	4735	Center	Closed system	10
	OW-2	No P_c	Anticline	4735	Center	Closed system	1
	OW-3	No P_c	Anticline	4735	Center	Closed system	5
	OW-4	No P_c	Anticline	4735	Center	Closed system	25
	OW-5	P_c	Anticline	4735	Center	Closed system	10
	OW-6	High P_c	Anticline	4735	Center	Closed system	10
	OW-7	P_c	Anticline	4735	Center	Aquifer	10
	OW-8	No P_c	Anticline	4735	Center	Aquifer	10
	OW-8	High P_c	Anticline	4735	Center	Aquifer	10
	OW-9	No P_c	Anticline	4700	Center	Closed system	10

Closed system: the no-flow condition implies zero superficial velocity at the outer boundary and hence the local pressure gradient must also be zero, that is, $\partial P_e/\partial r|_{r=r_e} = 0, t > 0$; aquifer: the well is situated in the center of a drainage area with a constant pressure, equal to the initial pressure, P_i, maintained along the outer boundary, $P(r_e, t) = P_i, t > 0$.

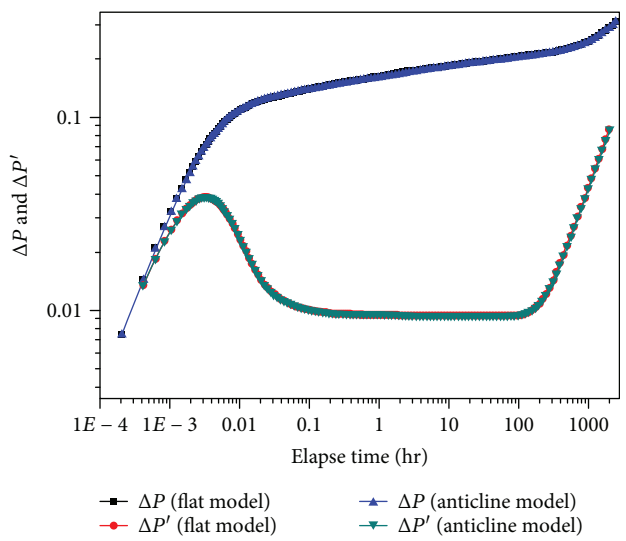

Figure 5: This figure shows the log-log plot of drawdown from closed system. It shows that the pressure responses ($\Delta P_0 = P_i - P_{wf}$) and the pressure derivative responses ($\Delta P_o'$) for anticline model and flat model under single-phase flow condition are the same.

Hence, the pressure derivative is a function of the flow rate changes with time in the reservoir.

Before pseudo-steady state is reached, the flow rate in the reservoir will continue to increase, for example, if $t < t_{pss}$, where t_{pss} is the time to reach the pseudo-steady state; we can get

$$\frac{\partial q_t\left(r', t\right)}{\partial t} > 0. \tag{9}$$

According to the result of (9), (8) shows that the pressure derivative will remain positive until the pseudo-steady state is reached, that is,

$$\frac{d\Delta P_o(t)}{d(\ln t)} > 0, \quad t < t_{pss}. \tag{10}$$

At late time, when the pressure disturbance reaches a closed boundary, the formation pressure decreases with time, until the drawdown at wellbore is equal to the drawdown at boundary, from then on, the pseudo-steady state flow will start.

At the same time, the formation flow rate at any location with elapsed time will approach to some constant value and the increment of changes for formation flow rate at any location will approach to zero, that is,

$$\Delta q_t\left(r', t\right) \to 0, \quad t \to t_{pss} \tag{11}$$

After the pseudo-steady state flow, the increment of changes for formation pressure at any location will approach to constant.

$$\Delta P_o(r, t) \to \text{constant}, \quad t \to t_{pss}, \tag{12}$$

$$\text{or } \frac{d\Delta P_o(t)}{d(\ln t)} \to \text{constant}^* t, \quad t \to t_{pss}. \tag{13}$$

Equation (13) indicates that in late time, the slope of derivative in log-log plot is unit 1. Figure 5 shows that the numerical result is identical to that from (13).

All of these results are consistent with single-phase flow solutions in closed system.

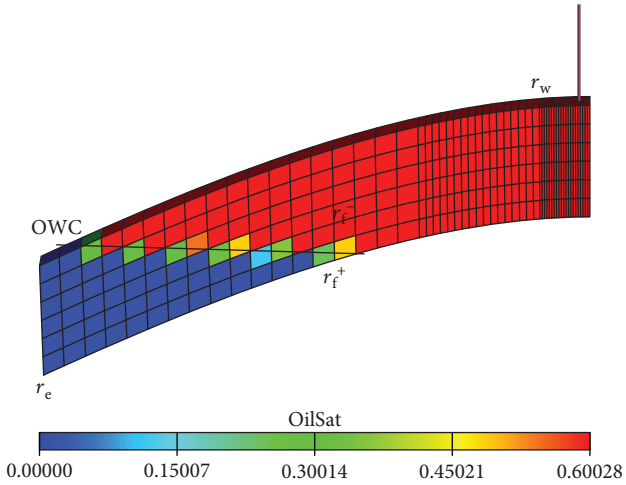

Figure 6: According to Buckley-Leverett theory, using saturation front, reservoir can be divided into three regions. The first region is between the wellbore and the downstream side of saturation front, $r_w < r < r_f^-$; the second region is between the downstream side of saturation front and the upstream side of saturation front, $r_f^- < r < r_f^+$; and the third region is between the upstream side of saturation front and outer boundary of the reservoir, $r_f^+ < r < r_e$.

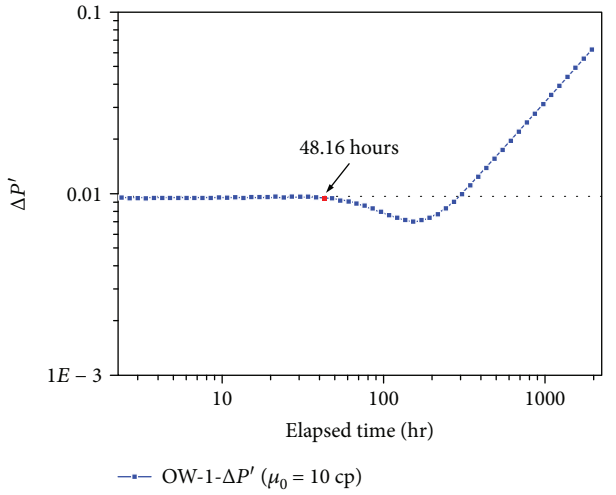

Figure 7: The log-log plot of drawdown of a closed system which shows that the pressure derivative starts to decrease at 48.16 hours. At this point, the pressure reached transition zone.

3.2.2. Two-Phase Flow. For two-phase flow in homogeneous reservoir, the capillary pressure was not considered at the beginning, that is, $P_o = P_w, P_c = 0$. According to Buckley-Leverett theory, in oil-water transition zone, there exists saturation front, and the reservoir can be divided into three regions (Figure 6). The first region is between the wellbore and the downstream side of saturation front, $r_w < r < r_f^-$; the second region is between the downstream side of saturation front and the upstream side of saturation front, $r_f^- < r < r_f^+$; and the third region is between the upstream side of saturation front and outer boundary of the reservoir, $r_f^+ < r < r_e$.

After the pressure reached the boundary of closed system and the pseudo-steady state occurred, the increment of change for volumetric flow rate at any location in late time will approach to zero, that is, $\Delta q_t(r', t) \to 0, t > t_{pss}$ or $(\partial \Delta q_t(r', t))/\partial t \to 0, t > t_{pss}$; the general pressure derivative equation (7) can be simplified as

$$\frac{d\Delta P_o(t)}{d \ln t} = \frac{t}{2\pi Kh}\left\{\int_{r_w}^{r_f^-}\left[-\frac{q_t(r',t)}{r'\lambda_t^2(r',t)}\frac{\partial \lambda_t(r',t)}{\partial t}\right]dr' + \int_{r_f^-}^{r_f^+}\left[-\frac{q_t(r',t)}{r'\lambda_t^2(r',t)}\frac{\partial \lambda_t(r',t)}{\partial t}\right]dr' + \int_{r_f^+}^{r_e}\left[-\frac{q_t(r',t)}{r'\lambda_t^2(r',t)}\frac{\partial \lambda_t(r',t)}{\partial t}\right]dr'\right\}. \quad (14)$$

Ahead of saturation front, the flow is single-phase (oil) and the total effective mobility is unchanged, so $d\lambda_t(t)/dt = 0$, $r_w < r < r_j^-$; from upstream of saturation front to outer boundary, the total effective mobility increases and finally becomes constant, so at late time, $d\lambda_t(t)/dt \to 0$, $r_f^+ < r < r_e$, then (14) can be reduced to

$$\frac{d\Delta P_o(t)}{d(\ln t)} = \frac{1}{2\pi Kh}\int_{r_f^-}^{r_f^+}\left[-\frac{q_t(r',t)}{r'\lambda_t^2(r',t)}\frac{\partial \lambda_t(r',t)}{\partial (\ln t)}\right]dr' = -\frac{t}{2\pi Kh}\int_{r_f^-}^{r_f^+}\left[\frac{q_t(r',t)}{r'\lambda_t^2(r',t)}\frac{\partial \lambda_t(r',t)}{\partial t}\right]dr'. \quad (15)$$

Equation (15) is the generalized pressure derivative equation for transition zone of oil-water or gas-water systems. Since (15) is a highly nonlinear equation and cannot obtain analytical solution, it can be used to qualitatively validate the numerical solution and interpret the pressure behavior in transient zone.

According to the interpretation results of numerical solution, the pressure derivative curve, the total mobility curve of saturation front, the fluid rate of saturation front, and the total mobility derivative curve of saturation front were obtained. As shown in Figure 7, the pressure derivative starts to go down at 48.16 hours, and then goes up. How can this phenomenon be explained? Figure 8 shows that when the well produces by depletion, at downstream saturation front, with oil produced, the combined water did not flow and the oil mobility was decreased, so the total mobility was decreased until to the point of 48.16 hours. At upstream saturation front, the combined water starts to flow, water encroachment will occur, and the total mobility starts to increase rapidly.

After 48.16 hours, the $\lambda_t(r, t)$ of upstream saturation front increases, so $\partial \lambda_t(r, t)/\partial t$ increases with time and $\partial \lambda_t(r, t)/\partial t > 0$ (Figure 9). According to (15), $d\Delta P_o(t)/d(\ln t)$ is negative and decreasing with time.

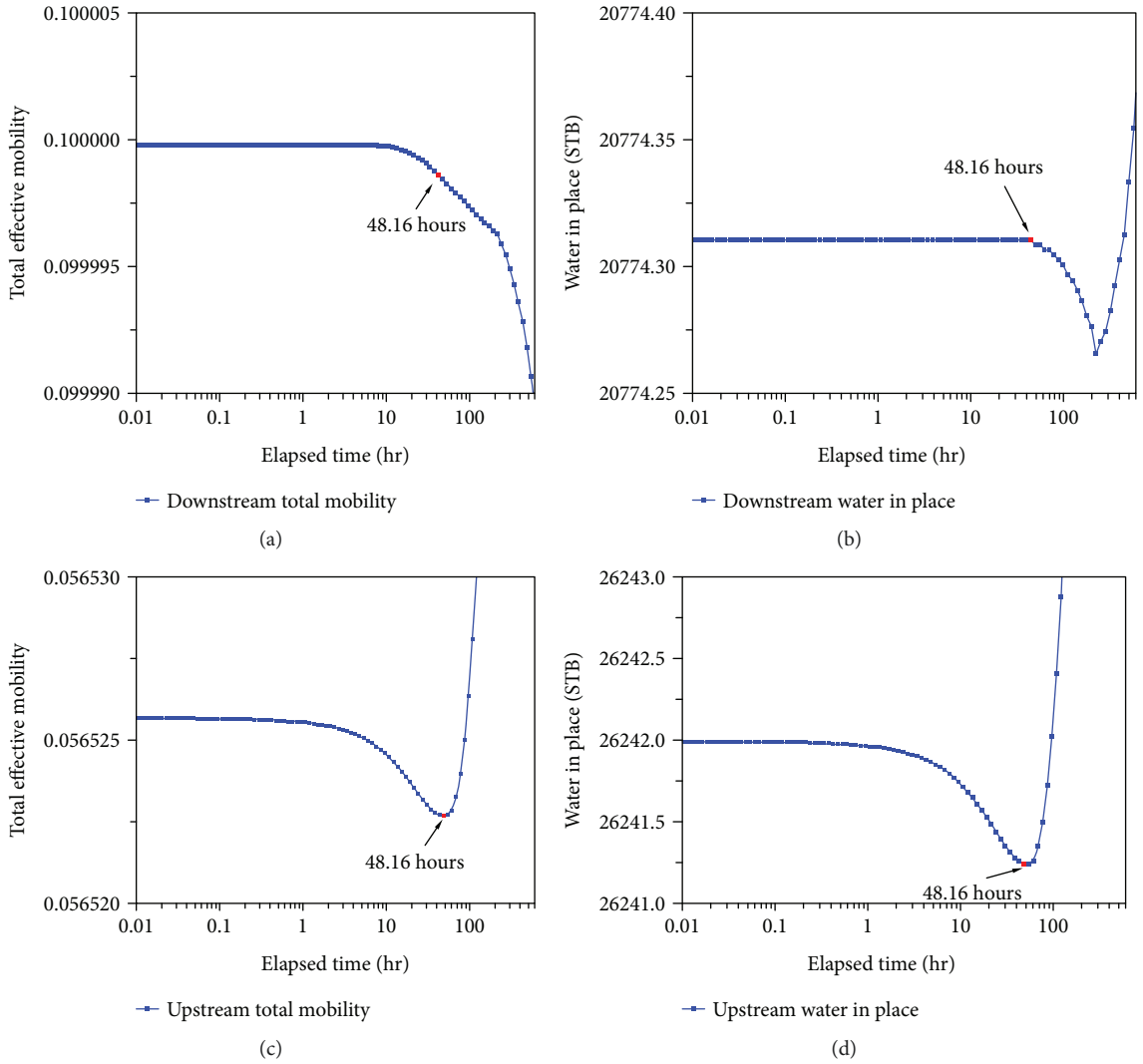

Figure 8: (a) The total mobility curve and (b) the volumetric of water curve just downstream of the saturation front ($r \to r_f^-$), before 48.16 hr, the combined water does not flow, but because the oil is moving, the total mobility decreases. (c) The total mobility curve and (d) the volumetric of water curve at upstream saturation front ($r \to r_f^+$), from 48.16 hr, the water encroachment will occur, the total mobility starts to increase rapidly.

3.2.3. Sensitivity Studies

(1) Effect of Different Oil-Water Contacts (OWC). Under different OWC conditions (as listed in Table 2, the depths of OWC for case OW-1 and OW-9 are 4735 ft and 4700 ft, resp.), there is a large variation in the pressure derivative. Figure 10 shows that the pressure derivatives go down overall at the transition zone, but for high oil-water contact, because the saturation front is much higher, the pressure disturbance reaches the saturation front quickly. Hence, the pressure derivative goes down earlier and much further.

(2) Effect of Capillary Pressure. In practice, capillary pressure exists everywhere in reservoirs with multiphase flow as long as oil saturation is different from water saturation [26–28]. This is reservoir's inherent nature. According to analysis above, considering the capillary pressure of saturation front in transition zone, (7) can be rearranged for transition zone as

$$\frac{d\Delta P_o(t)}{d(\ln t)} = \frac{t}{2\pi Kh}\int_{r_f^-}^{r_f^+}\left\{-\frac{q_t\left(r',t\right)}{r'\lambda^2{}_t\left(r',t\right)}\frac{\partial\lambda_t\left(r',t\right)}{\partial t}\right\}dr' + t\int_{r_f^-}^{r_f^+}\frac{\partial\lambda_{\text{equivalent}}\left(r',t\right)}{\partial t}\frac{\partial P_c\left(r',t\right)}{\partial S_w}\frac{\partial S_w\left(r',t\right)}{\partial r'}dr'. \tag{16}$$

For $\lambda_{\text{equivalent}}(r',t) = (\lambda_w(r',t))/(\lambda_t(r',t)) = (\lambda_w(r',t))/(\lambda_w(r',t) + \lambda_o(r',t)) = 1/(1 + (\lambda_o(r',t)/\lambda_w(r',t)))$, from the downstream saturation to the upstream saturation front ($r_f^- \to r_f^+$), $\lambda_w(r',t)$ increases with time and $\lambda_o(r',t)$

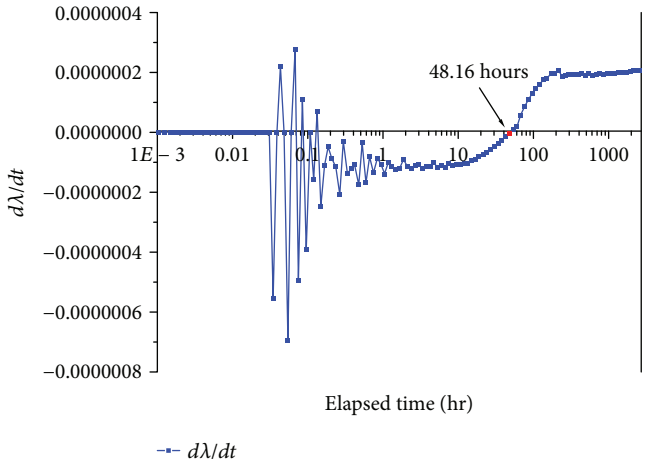

Figure 9: The total mobility derivative curve just upstream of the saturation front ($r \to r_f^+$); the total mobility derivative is positive and increasing with time (at early time, the calculation results are not stable due to numerical dispersion).

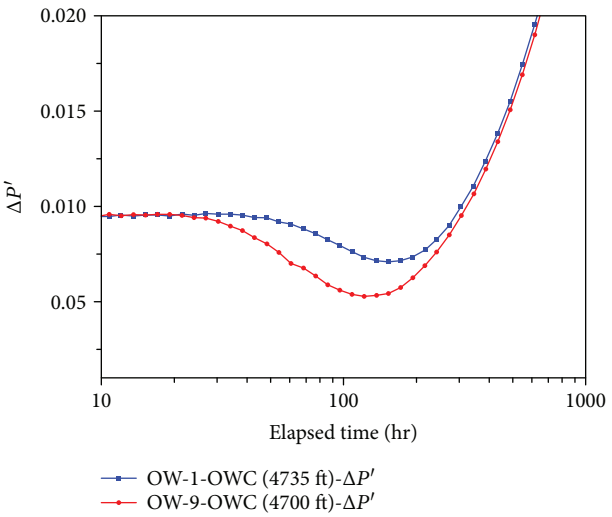

Figure 10: The log-log plot of drawdown for closed system. It shows that the pressure derivatives for different OWC cases all together go down in transition zone, but for high OWC case, the pressure derivative goes down in advance and much deeper.

decreases with time, so $\lambda_o(r', t)/\lambda_w(r', t)$ decreases with time. Hence, $\lambda_{equivalent}(r', t)$ increases and $\partial\lambda_{equivalent}(r', t)/\partial t > 0$. But for $\partial P_c(r', t)/\partial S_w$, it is negative as shown in Figure 3. However, Figure 11 indicates that $\partial S_w(r', t)/\partial r'$ is positive, so

$$\frac{\partial \lambda_{equivalent}\left(r', t\right)}{\partial t} \frac{\partial P_c\left(r', t\right)}{\partial S_w} \frac{\partial S_w\left(r', t\right)}{\partial r'} < 0. \quad (17)$$

Figure 12 shows that the transition zone pressure derivative of the reservoir with capillary pressure goes down more than that without capillary pressure.

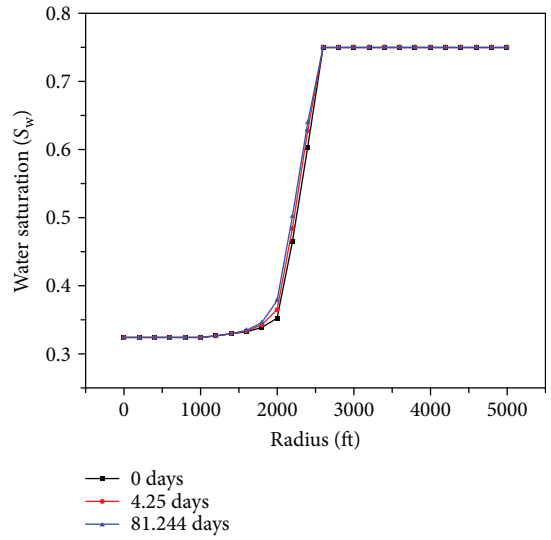

Figure 11: Water saturation profile changes with radial distance.

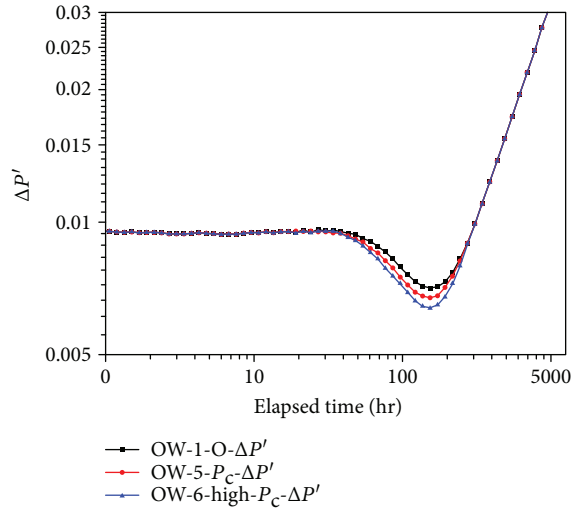

Figure 12: The log-log plot of drawdown of a closed system. It shows that the transition zone pressure derivative of reservoir with capillary pressure goes down more than that without capillary pressure.

(3) Effect of Constant Pressure Outer Boundary. As shown in Figure 13, with and without capillary pressure, the pressure derivative followed nearly the same trend in reservoir with constant pressure at the outer boundary.

(4) Effect of Oil Viscosity. In order to study the pressure behavior of a transition zone caused by varying oil viscosities, four cases were designed, in which oil viscosity is 1 cp, 5 cp, 10 cp, and 25 cp (the oil/water viscosity ratio is 2, 10, 20, and 50), respectively.

According to the radius of investigation equation,

$$R_{inv} = 0.033\sqrt{\frac{kt}{\phi\mu c_t}}. \quad (18)$$

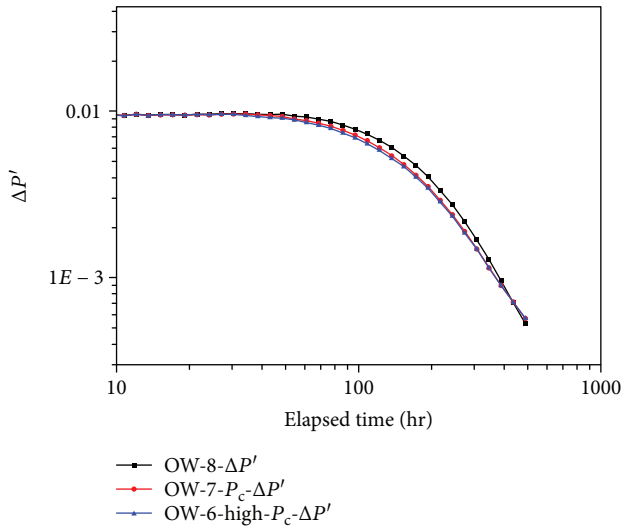

Figure 13: The log-log plot of drawdown in reservoir with constant pressure boundary. It shows that the transition zone pressure derivative of reservoir with capillary pressure goes down more than that without capillary pressure.

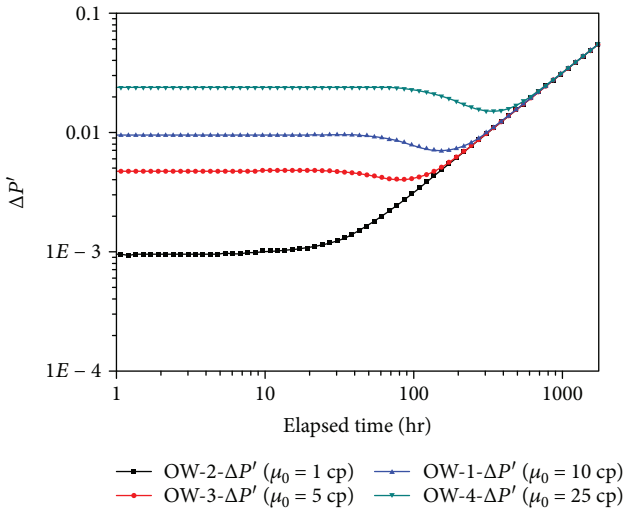

Figure 14: The log-log plot of pressure response in a reservoir without P_c under different oil viscosities. If oil viscosity is greater, the time that takes to reach the transition zone is longer.

If the oil/water viscosity ratio is higher, the time of the pressure reaching transition zone is longer. This is consistent with simulation results shown in Figure 14.

Meanwhile, according to numerical simulation results, under low oil/water viscosity ratio condition (such as the oil/water viscosity ratio is 2), the pressure derivative did not decrease in log-log plot. As shown in Figure 15, although the total mobility has changed, the changes of total mobility are very small, especially in late time, $\partial\lambda_t/\partial t \rightarrow$ constant; hence, the total effective mobility did not change quickly at saturation front of transition zone under low oil/water viscosity ratio condition, so the phenomenon of the pressure derivative going down at transition zone will not occur.

3.3. Case Study 2: Gas-Water System

3.3.1. Two-Phase Flow. For a gas-water reservoir system, there are two boundary system conditions: the closed boundary and the constant pressure boundary. Sensitivity studies were designed for these systems. The key parameters are listed in Table 3.

As with the studies of the oil-water system, capillary pressure was not considered at first. As shown in Figure 16, the pressure derivative of the wellbore pressure starts to go up at 10.10 hours. This is due to the rapid decrease in total mobility (Figure 17). According to (7), at 10.10 hours, the $\lambda_t(r,t)$ decreased, so the absolute value of $\partial\lambda_t(r,t)/\partial t$ increased and $\partial\lambda_t(r,t)/\partial t < 0$, but $d\Delta P_o(t)/d \ln t$ is positive and increasing with time.

3.3.2. Sensitivity Studies

(1) Effect of Capillary Pressure. According to (18), because $-(q_t(r',t)/r'\lambda^2{}_t(r',t))(\partial\lambda_t(r',t)/\partial t) > 0$, $(\partial\lambda_{\text{equivalent}}(r',t)/\partial t)(\partial P_c(r',t)/\partial S_w)(\partial S_w(r',t)/\partial r') > 0$, so $(d\Delta P_o(t))/(d \ln t) > 0$.

Figure 18 shows that the transition zone pressure derivative of a reservoir with capillary pressure goes up more than that without capillary pressure.

(2) Effect of Constant Pressure Boundary. Considering constant pressure boundary, Figure 19 shows the simulation results of drawdown (DD) test and buildup (BU) test under constant pressure boundary conditions. The pressure derivatives of DD and BU both go up when the pressure reached transition zone.

Figure 20 shows that the transition zone pressure derivative in a reservoir with capillary pressure goes up more than that without capillary pressure.

(3) Distance of Movement for Saturation Front. In order to simulate the saturation front movement, PDG data were generated by simulation (Figure 21). The first DD test and the last DD test were selected for analysis. As shown in Figure 22, for the first DD, at 2.123 hours, the pressure reached the saturation front, but for the last DD, the time for pressure reaching the saturation front is about 1.190 hours. Using (18), for the first DD, the radius investigation of R_1 is calculated as about 1712.237 ft; for the last DD, the radius investigation of R_2 is calculated as about 2282.869 ft. The angle of formation bedding (α) is about 2.8°, $H = \sin\alpha \times (R_2 - R_1)$; the height of saturation front can be obtained as about 27.87 ft. Figure 23 shows that the height of saturation front is about 27.7 ft. In comparison with the well test and simulation results, the error is only 0.6%.

4. Field Application

In order to apply the pressure behavior of the study in practice, two field examples are studied: a gas well test and an oil well test.

4.1. Well A: Gas Well Test. This well is located between two faults. The distances from the well to the faults are 2100 ft and 3600 ft (Figure 24). The average permeability of the gas

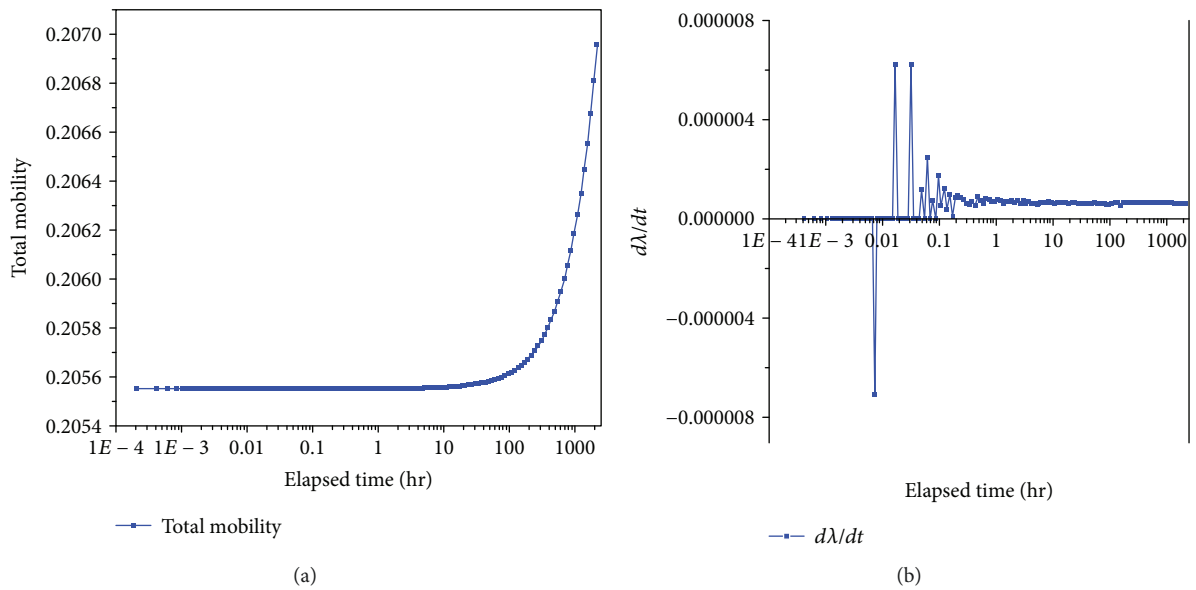

Figure 15: (a) The total mobility curve and (b) the total mobility derivative curve at upstream saturation front with oil viscosity at 1 cp. Although the total mobility has some changes, the total mobility derivative is very small and close to constant in late time.

Table 3: The design of different flow conditions.

Fluid	Case	P_c	Model	OWC (ft)	Well location	Aquifer	Viscosity (cp)
Gas-water model	GW-1	No P_c	Anticline	4735	Center	No	0.02
	GW-2	P_c	Anticline	4735	Center	No	0.02
	GW-3	P_c	Anticline	4735	Center	Aquifer	0.02
	GW-4	No P_c	Anticline	4735	Center	Aquifer	0.02
	GW-5	High P_c	Anticline	4735	Center	Aquifer	0.02

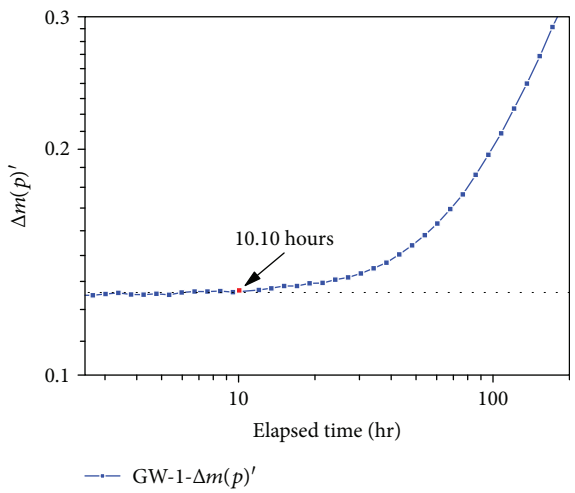

Figure 16: The log-log plot of gas-water reservoir with closed boundary. The pressure derivative starts to increase from 10.10 hours ($m(p)$ is pseudopressure of gas-water reservoir, $\Delta m(p) = m(P_i) - m(P_{wf})$, $\Delta m(p)' = d\Delta m(p)/d \ln(t)$).

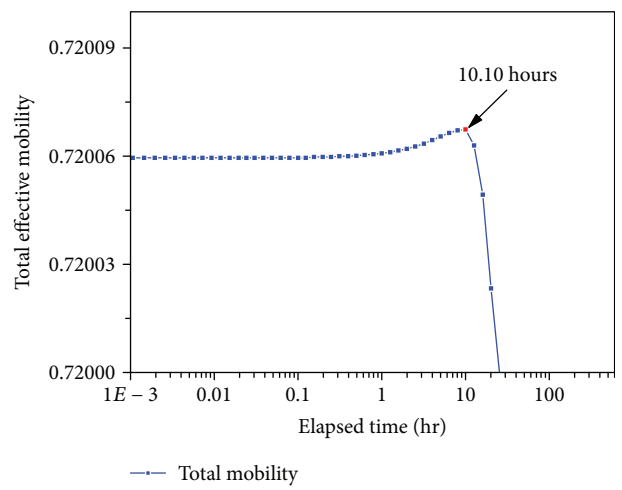

Figure 17: The total mobility curve at upstream saturation front ($r \to r_f^+$), from 10.10 hours. The total mobility starts to decrease rapidly.

reservoir is 1.8 mD, and the porosity is 11.5%. In order to test well productivity, a well test was performed (Figure 25). From the test data, the last build up data was analyzed.

Because geologist engineers thought that the gas well did not encounter a water layer during the drilling, this gas reservoir is assumed to be a dry gas reservoir. Therefore, a single-phase theory was used to interpret the well test.

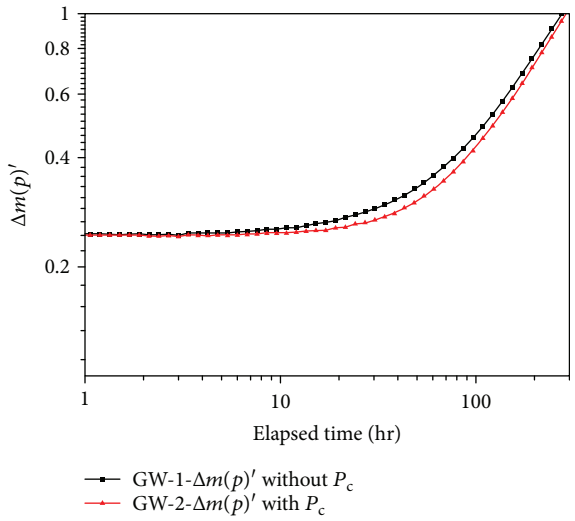

Figure 18: The log-log plot of the pressure response in gas-water reservoir with P_c and closed boundary. The pressure derivative with capillary pressure goes up more than that without capillary pressure.

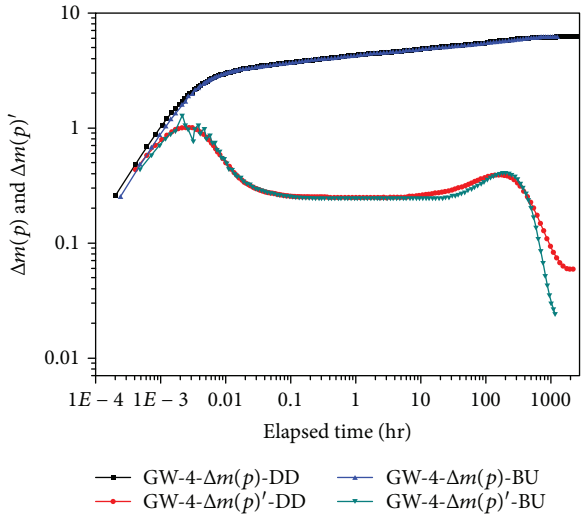

Figure 19: The log-log plot of the pressure response in gas-water reservoir under constant pressure boundary. The pressure derivative of DD and BU goes up when the pressure reached transition zone and then goes down when the pressure reached outer boundary.

From the log-log plot (Figure 26), at late time, the pressure derivative went up, using one fault model to match this test response; at 670 ft away from well A, there is a no-flow boundary. Combining the geological knowledge, reservoir engineers believed this no-flow boundary may be a subseismic fault. But after this well was put into production for two months, the water broke through.

The lesson learnt from this case was that the use of single-phase theory to interpret the test is inappropriate. Although well test data had some ambiguities, if the impact of multiphase flow was not taken into account, especially at transition zone, which can affect the late time pressure response, the analysis result could lead to a completely wrong decision. In fact, in this well test log-log plot, the pressure derivative goes up at late time, purely due to the changes of total mobility in transition zone, and nothing to do with the reservoir outer boundary.

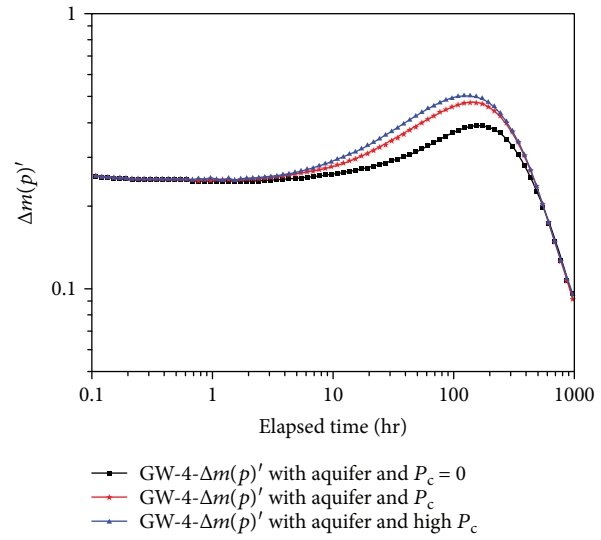

Figure 20: The log-log plot of the pressure response in gas-water reservoir with P_c and constant pressure boundary. It shows that the pressure derivative with capillary pressure goes up more than that without capillary pressure in transition zone.

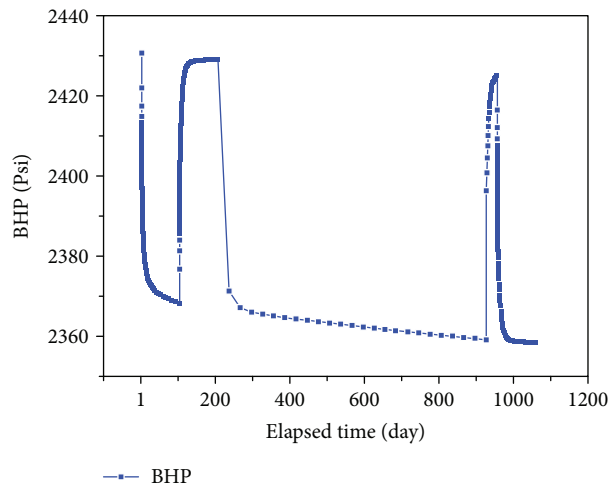

Figure 21: The bottom-hole pressure history. The first DD and last DD were selected for the analysis.

4.2. Well B: Oil Well Test. This reservoir is an anticline reservoir (Figure 27). The average buried depth of this reservoir is 1650 ft, and the oil viscosity is 120 cp. But the average permeability of the formation is 3 D, and the porosity is 0.27. Hence, although oil property is very bad, the formation property is very good. Using conventional method to produce, the single well productivity is very high. The key of the field development is the evaluation of formation energy. So well

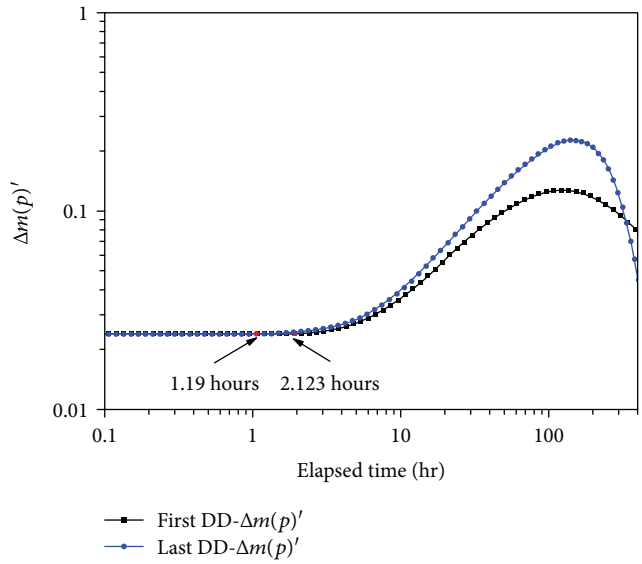

Figure 22: The interpretation result of the first DD and last DD. For the first DD, from 2.123 hours, the pressure reaches saturation front, but for the last DD, the time of pressure reaching saturation front is about 1.190 hours.

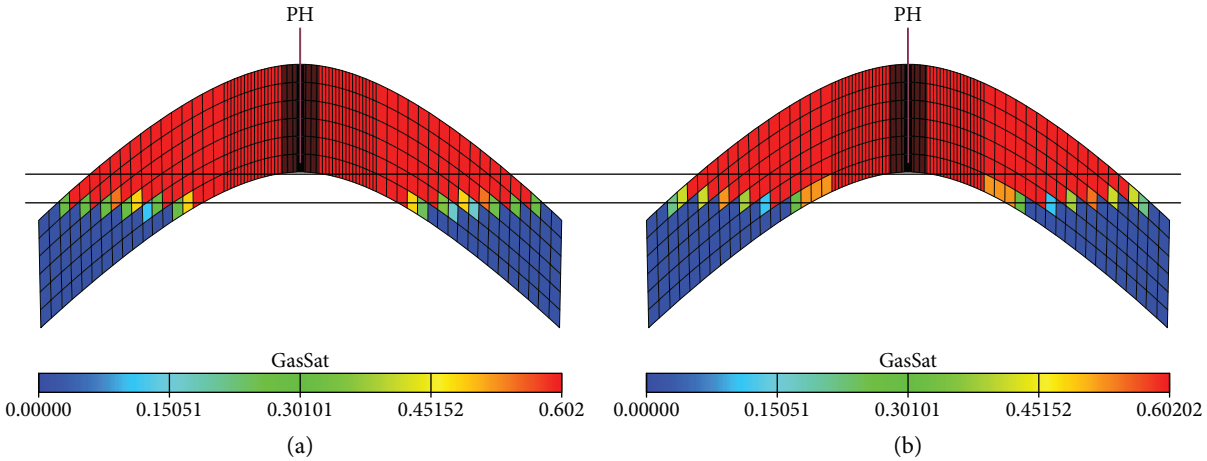

Figure 23: (a) The initial oil-water contact (OWC). (b) The oil-water contact at 1060 days, according to the saturation profile. The distance of movement for saturation front with time is about 27.7 ft.

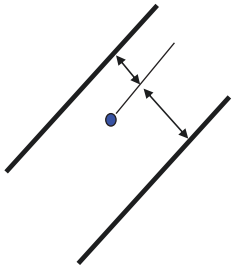

Figure 24: The sketch map of well A. This gas reservoir was controlled by two faults.

testing was used (Figure 28). From the test data, the last DD and the last BU were selected for the analysis. The DD and BU plots show that at late time, the pressure derivatives all go down (Figures 29 and 30), which was a sign of the pressure reaching aquifer, and it means that the reservoir has higher energy.

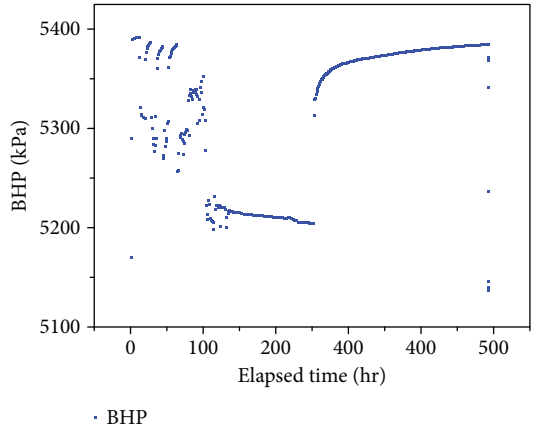

Figure 25: The test history of well A. The last BU was selected for the analysis.

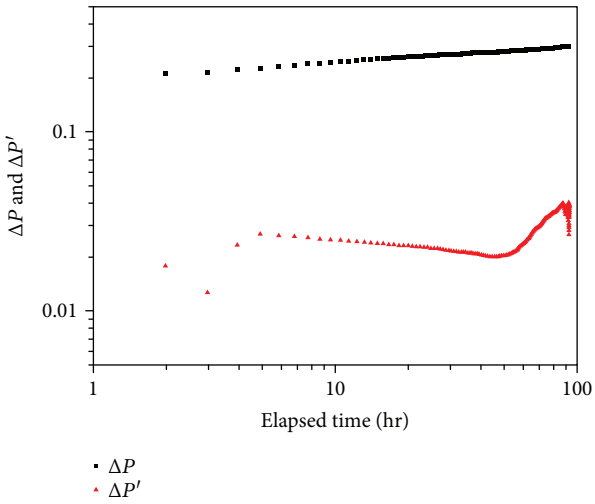

Figure 26: The log-log plot of well A last BU. At late time, the pressure derivative goes up.

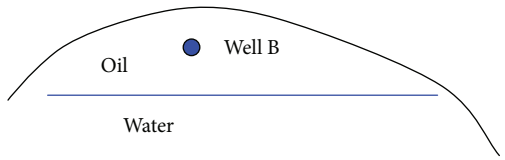

Figure 27: The plan view of well B. This oil reservoir is an anticline reservoir.

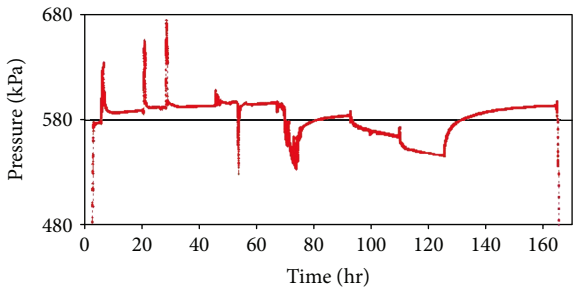

Figure 28: The test history of well B. The last DD and last BU are selected for analysis.

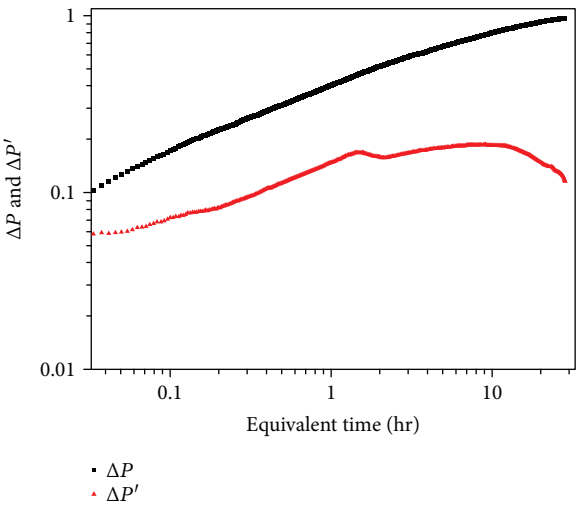

Figure 29: The log-log plot of well B last DD. From this plot, the pressure derivative decreases at late time.

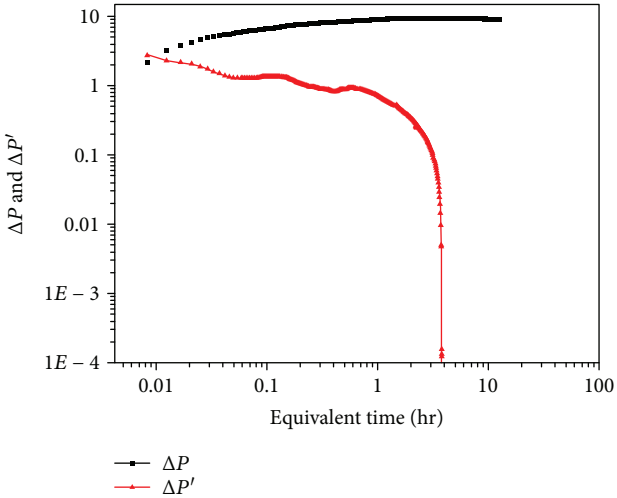

Figure 30: The log-log plot of well B last BU. On this plot, the pressure derivative also decreases quickly at late time.

According to the well testing result, at early development phase, the natural depletion mechanism development was advised. But after 6-month production, some wells in this reservoir could not continue production, including well B.

In fact, for this reservoir, if multiphase flow theory was used to interpret the well test, in the log-log plot of DD, the pressure derivative decreased, purely as a response to the change of the total mobility in the transition zone. Again, this is nothing to do with the outer boundary.

5. Conclusions

(1) Based on a theoretical development by Thompson, a new expression can be derived from Darcy's law. According to this expression and the numerical well test results, we reasonably interpret the pressure behavior of transition zone in oil-water and gas-water reservoirs. The results presented in this work are generally applicable to multiphase reservoir, which have either an infinite-acting or a constant pressure outer boundary.

(2) Capillary pressure in the transition zone has an insignificant impact on pressure response.

(3) Two field examples were interpreted, based on this new understanding of pressure behavior in the transition zone. It seems to work well as an explanation of the situations of these two well tests.

Nomenclature

q_t: Total rate in RB/D for all systems

q_o: Oil rate in RB/D for all systems
q_w: Water rate in RB/D for all systems
K: Absolute reservoir permeability, mD
K_{ro}: Oil relative permeability
K_{rw}: Water relative permeability
K_{rg}: Gas relative permeability
μ_0: Oil phase viscosity, cp
μ_w: Water phase viscosity, cp
μ_g: Gas phase viscosity, cp
$A(r)$: Cross-sectional area, ft^2
P_c: Capillary pressure, psi
P_o: Oil phase pressure, psi
P_w: Water phase pressure, psi
P_{wf}: Flowing bottom-hole pressure, psi
H: Distance of movement for saturation front with time, ft
α: The angle of bedding, °
R_{inv}: Investigation radius, ft
r: Radius, ft
r_w: Wellbore radius, ft
r_f^-: Radius to downstream saturation front, ft
r_f^+: Radius to upstream saturation front, ft
r_e: Radial extent of reservoir, ft
S_w: Water saturation, fraction
h: Formation thickness, ft
λ_o: Oil phase effective mobility
λ_w: Water phase effective mobility
λ_t: Total effective mobility
t: Time, hour
t_{pss}: Pseudo-steady state time, hr
R_{inv}: Investigation radius, ft
ϕ: Porosity
c_t: Total compressibility, psi^{-1}.

Data Availability

The data used to support the findings of this study are available from the corresponding author upon request.

Disclosure

It should be noted that this article is part of the results of the Wenbin Xu's doctorate.

Conflicts of Interest

The authors declare no conflict of interest.

Authors' Contributions

Each author has made contributions to the present paper. Wenbin Xu conceived, designed, and performed the simulations. Zhihui Liu and Jie Liu processed and analyzed the simulation data, and Yongfei Yang analyzed the simulation data and provided general supervision. All authors have read and approved the final manuscript.

Acknowledgments

The authors would like to express appreciation to the following financial support: the National Natural Science Foundation of China (nos. 51674280, 51711530131, and 51490654), Key Research and Development Plan of Shandong Province (2018GSF116009), Applied Basic Research Projects of Qingdao Innovation Plan (16-5-1-38-jch), Fundamental Research Funds for the Central Universities (no. 17CX05003), National Science and Technology Major Project (2016ZX05010002005), and Program for Changjiang Scholars and Innovative Research Team in University (IRT_16R69).

References

[1] K. A. Culligan, D. Wildenschild, B. S. B. Christensen, W. G. Gray, M. L. Rivers, and A. F. B. Tompson, "Interfacial area measurements for unsaturated flow through a porous medium," *Water Resources Research*, vol. 40, no. 12, 2004.

[2] P.-E. Danielsson, "Euclidean distance mapping," *Computer Graphics and Image Processing*, vol. 14, no. 3, pp. 227–248, 1980.

[3] S. Elkatatny, M. Mahmoud, and H. A. Nasr-El-Din, "Filter cake properties of water-based drilling fluids under static and dynamic conditions using computed tomography scan," *Journal of Energy Resources Technology*, vol. 135, no. 4, article 042201, 2013.

[4] Z. Jiang, K. Wu, G. Couples, M. I. J. van Dijke, K. S. Sorbie, and J. Ma, "Efficient extraction of networks from three-dimensional porous media," *Water Resources Research*, vol. 43, no. 12, pp. 2578–2584, 2007.

[5] Z. T. Karpyn, M. Piri, and G. Singh, "Experimental investigation of trapped oil clusters in a water-wet bead pack using X-ray microtomography," *Water Resources Research*, vol. 46, no. 4, 2010.

[6] T. Y. Kong and A. Rosenfeld, "Digital topology: introduction and survey," *Computer Vision, Graphics, and Image Processing*, vol. 48, no. 3, pp. 357–393, 1989.

[7] C. Lu, J. Wang, C. Zhang et al., "Transient pressure analysis of a volume fracturing well in fractured tight oil reservoirs," *Journal of Geophysics and Engineering*, vol. 14, no. 6, pp. 1509–1520, 2017.

[8] F. Dongyan, Y. Jun, S. Hai, Z. Hui, and W. Wei, "A composite model of hydraulic fractured horizontal well with stimulated reservoir volume in tight oil & gas reservoir," *Journal of Natural Gas Science and Engineering*, vol. 24, no. 5, pp. 115–123, 2015.

[9] S. Wang, Q. Feng, and X. Han, "A hybrid analytical/numerical model for the characterization of preferential flow path with non-Darcy flow," *PLoS One*, vol. 8, no. 12, article e83536, 2013.

[10] Q. Feng, S. Wang, W. Zhang, Y. Song, and S. Song, "Characterization of high-permeability streak in mature waterflooding reservoirs using pressure transient analysis," *Journal of Petroleum Science and Engineering*, vol. 110, pp. 55–65, 2013.

[11] M. Wu, M. Ding, J. Yao, S. Xu, L. Li, and X. Li, "Pressure transient analysis of multiple fractured horizontal well in composite shale gas reservoirs by boundary element method," *Journal of Petroleum Science and Engineering*, vol. 162, no. 3, pp. 84–101, 2018.

[12] Y. Yang, J. Yao, C. Wang et al., "New pore space characterization method of shale matrix formation by considering organic and inorganic pores," *Journal of Natural Gas Science and Engineering*, vol. 27, Part 2, pp. 496–503, 2015.

[13] H. Geistlinger, S. Mohammadian, S. Schlueter, and H. J. Vogel, "Quantification of capillary trapping of gas clusters using X-ray microtomography," *Water Resources Research*, vol. 50, no. 5, pp. 4514–4529, 2014.

[14] A. Georgiadis, S. Berg, A. Makurat, G. Maitland, and H. Ott, "Pore-scale micro-computed-tomography imaging: nonwetting-phase cluster-size distribution during drainage and imbibition," *Physical Review E*, vol. 88, no. 3, article 033002, 2013.

[15] M. M. Kamal, S. Morsy, F. Suleen et al., "Determination of insitu reservoir absolute permeability under multiphase flow conditions using transient well testing," in *SPE Annual Technical Conference and Exhibition*, Houston, TX, USA, 2015.

[16] S. Chen, G. Li, A. M. Peres, and A. C. Reynolds, "A well test for in-situ determination of relative permeability curves," *SPE Reservoir Evaluation & Engineering*, vol. 11, no. 1, pp. 95–107, 2013.

[17] A. T. Krummel, S. S. Datta, S. Münster, and D. A. Weitz, "Visualizing multiphase flow and trapped fluid configurations in a model three-dimensional porous medium," *AICHE Journal*, vol. 59, no. 3, pp. 1022–1029, 2013.

[18] T. S. Ramakrishnan and D. J. Wilkinson, "Formation producibility and fractional flow curves from radial resistivity variation caused by drilling fluid invasion," *Physics of Fluids*, vol. 9, no. 4, pp. 833–844, 1997.

[19] R. D. Roadifer, "Pressure behavior of wells completed in multiphase reservoirs containing a constant pressure boundary," in *Proceedings of SPE Annual Technical Conference and Exhibition*, Denver, CO, 1996.

[20] S. Wang and B. Yu, "Study of the effect of capillary pressure on the permeability of porous media embedded with a fractal-like tree network," *International Journal of Multiphase Flow*, vol. 37, no. 5, pp. 507–513, 2011.

[21] K. A. Culligan, D. Wildenschild, B. S. B. Christensen, W. G. Gray, and M. L. Rivers, "Pore-scale characteristics of multiphase flow in porous media: a comparison of air–water and oil–water experiments," *Advances in Water Resources*, vol. 29, no. 2, pp. 227–238, 2006.

[22] J. Ghosh and G. R. Tick, "A pore scale investigation of crude oil distribution and removal from homogeneous porous media during surfactant-induced remediation," *Journal of Contaminant Hydrology*, vol. 155, pp. 20–30, 2013.

[23] A. M. Dahroug, J. W. Baily, and S.-Y. Zheng, "The application of transient pressure testing to track phase boundaries during production - a one well case study from UKSC," in *Proceedings of SPE Europec/EAGE Annual Conference*, Madrid, Spain, 2005.

[24] G. Eigestad and J. Larsen, "Numerical modelling of capillary transition zones," in *Proceedings of SPE Asia Pacific Oil and Gas Conference and Exhibition*, Brisbane, Australia, 2000.

[25] J. R. Fanchi, R. L. Christiansen, and M. J. Heymans, "Estimating oil reserves of fields with oil/water transition zones," *SPE Reservoir Evaluation & Engineering*, vol. 5, no. 4, pp. 311–316, 2013.

[26] S. Iglauer, M. A. Fernø, P. Shearing, and M. J. Blunt, "Comparison of residual oil cluster size distribution, morphology and saturation in oil-wet and water-wet sandstone," *Journal of Colloid and Interface Science*, vol. 375, no. 1, pp. 187–192, 2012.

[27] S. M. Hassanizadeh and W. G. Gray, "Mechanics and thermodynamics of multiphase flow in porous media including interphase boundaries," *Advances in Water Resources*, vol. 13, no. 4, pp. 169–186, 1990.

[28] S. Iglauer, M. Sarmadivaleh, C. Geng, and M. Lebedev, "In-situ residual oil saturation and cluster size distribution in sandstones after surfactant flooding imaged with X-ray micro-computed tomography," in *International Petroleum Technology Conference*, Doha, Qatar, 2014.